Materials Research. 2023; 26:e20220326
DOI: https://doi.org/10.1590/1980-5373-MR-2022-0326

Performance of EPDM Composites Under Thermal Plasma Ablative Tests

F. S. Miranda[a], E. S. P. Prado[a,b], R. J. Silva[a], A. M. Ribeiro[a], F. R. Caliari[a,d], F. L. Calciolari[c], A. S. Silva Sobrinho[a], G. Petraconi[a]*

[a]*Instituto Tecnológico de Aeronáutica (ITA/DCTA), Laboratório de Plasmas e Processos (LPP), São José dos Campos, SP, Brasil.*
[b]*Instituto Nacional de Pesquisas Espaciais (INPE), São José dos Campos, SP, Brasil.*
[c]*AVIBRAS Indústria Aeroespacial S/A, São José dos Campos, SP, Brasil.*
[d]*Center for Thermal spray Research at Stony Brook University, New York, USA*

Received: July 19, 2022; Revised: June 23, 2022; Accepted: November 30, 2022

In this work, a thermal plasma-based ablation test system was used to evaluate the ablative performance of the EPDM composite. The system produces a high enthalpy plasma jet generated by a plasma (DC) torch, operating at atmospheric pressure using compressed air as working gas, enabling the variation of the thermal flux concerned with the studied EPDM composites. The samples were characterized using Scanning Electron Microscopy (SEM), Energy Dispersive Spectroscopy (EDS), Fourier-Transform Infrared spectroscopy (FTIR), and Thermogravimetric Analysis (TGA) to investigate the morphology, mass-loss rate, the reaction layer (char formation), and chemical changes of the samples for each thermal flux. For a complete evaluation, the thermal fluxes were varied in 0.30, 0.45, 0.60, 0.75, and 0.90 MW/m^2 and for each thermal flux, disk-shape samples remained exposed to the plasma jet for 10s. During the plasma jet exposure time, the temperatures of the surface and the back of the samples were collected to verify the formed char layer's insulator capacity and the samples' thermal diffusivity for each experimental condition. The mass loss is continuous under the thermal fluxes of 0.30 and 0.45 MW/m^2, stabilizing at 60% until 0.75 MW/m^2. The formed char layer begins to lose its protective capacity, evidenced by the size decrease (from 800 μm to 700 μm), due to the ablation process of the reaction layer from the thermal flux of 0.90 MW/m^2.

Keywords: *Thermal Plasma, EPDM composite, Ablation, Reaction layer.*

1. Introduction

Ethylene propylene diene monomer (EPDM) composite is a type of carbonized ablation material; its low density, high elongation, and good ablation resistance have led to its wide application as internal insulation in solid rocket motors (SRMs)[1-3]. Additionally, EPDM possesses the lowest density among elastomers (0.85 g/cm^3); this is an essential property; for these reasons, EPDM is the ideal candidate matrix for elastomeric ablatives[4-6]. EPDM rubber is a non-crystalline reinforcement rubber showing low mechanical strength, making it necessary to use reinforcement agents such as silica to improve its mechanical properties[4,7-10]. Fillers are used to reducing the thermal conductivity of materials and improve their insulation effects under the action of high-temperature gas, improve the integrity and robustness of the char layer, and protect the insulation from erosion by gas and particles, thereby reducing the ablation rate[8,11-13]. In this context, the addition of reinforcements in EDPM, such as the aramid fibres, was often used due to its low density, high thermal capacity, chemical stability, fire, and ablation resistance[1,2,7,14].

There are complex phenomena involved in the ablation process of materials, such as thermo-mechanical, thermo-physical, thermochemical ablation, and high-speed heat flow. These characteristics promote extremely high pressures and temperatures which decompose and erode the materials, enhancing their mass loss[15-17].

Nevertheless, the dripping and bending behaviours of EPDM composites make them lose their thermal protection function and even ignite other flammable materials; these are the most severe drawbacks of using EPDM as a thermal protection material. Thus, it is necessary to develop an EPDM composite with self-supporting and anti-dripping properties[18-20]. When EPDM is exposed at high temperatures, a hard porous char layer can be formed. The char layer's formation helps reduce erosion and create a barrier for hot gases, whose morphology and strength play a crucial role in ablative resistance. Although, if the thermal effort is maintained, this layer will be consumed, and the heat is gradually transferred to the inner layer, creating a cascade effect until the material is entirely consumed[12,21,22]. Therefore, a dense, considerable inert, high-strength char layer is of interest to ensure excellent erosion resistance. Aiming these properties, fibres, ceramic fillers, flame retardants, phenolic resins, carbon nano-fillers, and the like are applied in the EPDM (forming a composite material) to improve the integrity and quality of the char layer[12,23,24]. For example, when the use of silicon-based materials as a filler, once

*e-mail: mirannda.fs@gmail.com

when the oxidation of Silicon (Si) occurs the formation of Silica (SiO_2) gives extra protection due to the self-healing characteristics and low oxygen permeability, which could seal the cracks and at the same time prevent the diffusion of oxygen to EPDM material[24,25].

However, ablation tests performed with oxyacetylene torches do not respond to all the degradation effects caused during EPDM application[26,27]. An approach that fits and can respond to almost all of the physicochemical effects promoted during the materials ablation process is the application of thermal plasma through plasma torches[28,29]. The high temperature and the high reactivity due to free ions and radicals make the plasma a powerful medium to promote chemical reactions. When considering plasmas which use compressed air as working gas, the oxidation process is more intense, being extremely important for ablative tests[30]. Thermal plasma is initiated when electrons are accelerated between two electrodes in a gaseous environment. The collision between electrons and larger particles becomes more frequent; these collisions transfer the kinetic energy of the electron, and the recombination of charged particles raises the temperature of the gas[31]. These characteristics ensure the simulation of an environment very close to the reality of applying materials exposed to high temperatures and high reactivity[32].

This work performed ablative tests in different thermal fluxes (0.30, 0.45, 0.60, 0.75, and 0.90 MW/m^2) in EPDM/Aramid/SiO_2 composite using a thermal plasma torch. The performance of the EPDM composite in ablative tests was evaluated by its morphology mass loss rate, characterization of the reaction layer (char formation), and chemical changes of the samples for each thermal flux.

2. Materials and Methods

2.1. EPDM samples

The EPDM composite was developed by Avibras Aerospace Industry S.A. Its composition will not be presented herein to preserve the company's intellectual property. The samples were prepared in disks of 12mm in diameter and 4 mm in thickness for the ablative tests using thermal plasma.

A typical chemical structure of EPDM is presented in Figure 1; some fillers and reinforcements could be added to this structure, such as aramid, SiO_2, polyurethane, polyamide and others.

2.2. Ablation tests

The experimental system comprises a thermal plasma torch, cooling system, DC electric power source, gas supply, and sample holder. For the ablation tests, the operation parameters of the plasma torch were fixed at the current of 100 A and voltage of 380 V (38 kW), with an air working gas flow rate of 180 L/min.

The exposure time of the samples was fixed at 10 seconds, and the heat flux was varied according to the standoff distance between the sample and the nozzle of the plasma torch.

The EPDM composite was characterized using Scanning Electron Microscopy (SEM) coupled with Energy Dispersive Spectroscopy (EDS) (Tescan, Vega 3 XMU) and Fourier-transform infrared spectroscopy (FTIR) (Perkin Elmer, Frontier) in ATR mode with 32 accumulations, to investigate the morphology, and chemical changes, the reaction layer (char formation), and mass-loss rate of the samples for each thermal flux.

Figure 2 shows the schematic drawing of the ablation system and the distances with its thermal fluxes.

2.3. Determination of thermal flows of the ablation tests

The linear calorimeter technique was used to calculate the thermal flows (of the plasma jet), which were directly exposed to the plasma jet of the torch. The calorimeter (Figure 3) consists of a cylindrical copper disk with a thickness of 3 mm and a diameter of 10mm fixed to support; the temperature measurements were made in situ using a type K thermocouple connected to a temperature data

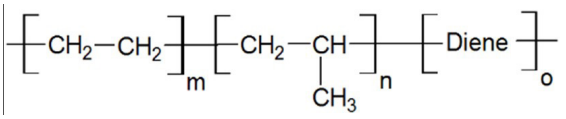

Figure 1. Chemical structure of EPDM rubber.

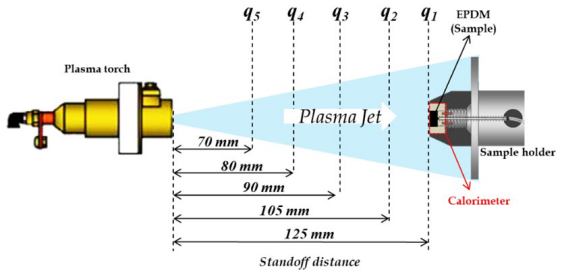

Sample	Thermal Flux (MW/m^2)
EPDM 1	q_1 = 0.30
EDPM 2	q_2 = 0.45
EPDM 3	q_3 = 0.60
EPDM 4	q_4 = 0.75
EPDM 5	q_5 = 0.90

Figure 2. Schematic drawing of the ablation system and the distances with thermal flows.

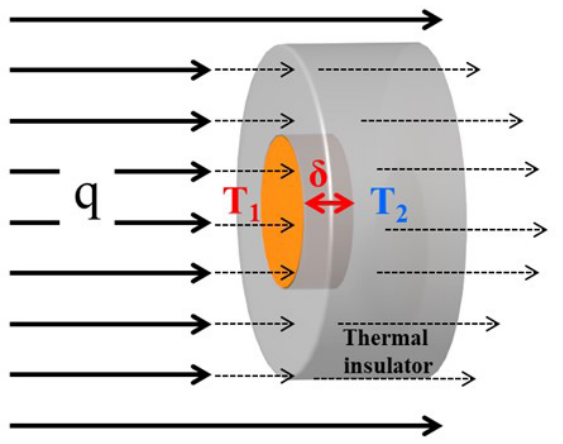

Figure 3. Schematic drawing of the calorimeter.

acquisition system, model ICP COM I-7000 series control modules[30]. The temperature measurements were acquired (with an output signal of 4 – 20mA) through the interface with a central processing unit, which enables the calculation of the heat flux through the calorimeter.

Copper was chosen due to the thermal conductivity and diffusivity already established in the literature. In these measurements, the thermal flow of the plasma jet focuses only on the surface of the calorimeter; the rest of the calorimeter is protected by a thermal insulator.

The temperature T1 is obtained from the incident surface of the plasma jet, and the temperature T2 is obtained at the back of the calorimeter. After a stabilization time, the temperature rise becomes linear, and the temperature difference between the plasma jet incidence surface and the back of the calorimeter becomes constant. Therefore, temperatures acquired (experimentally), the copper conductivity and diffusivity enable the calculation of thermal flow (q) by Equation 1[30], where the conduction mechanism makes the heat transfer:

$$q = \frac{\lambda}{\alpha}\delta\frac{dT}{dt} \quad \left(\frac{MW}{m^2}\right) \qquad (1).$$

where T is the temperature (K), α is the thermal diffusivity, λ is the thermal conductivity, and δ is the calorimeter thickness. The theoretical values of copper diffusivity and thermal conductivity considered for the calculation were $\alpha = 1.123E^{-4}$ (m^2/s) and $\lambda = 369$ (W/mK).

3. RESULTS AND DISCUSSION

3.1. Thermogravimetric analysis (TGA)

EPDM composite was initially submitted to thermogravimetric analysis using a Simultaneous thermal analyzer (Netzsch, Jupiter STA 449 F3). The main objective was to evaluate the sample's thermal stability, oxidation resistance, and mass loss rate under a controlled atmosphere. The analysis was carried out by setting the max temperature of 1000°C, with 10°C of the heating ramp and synthetic air (20% oxygen and 80% nitrogen) as a working gas (oxidant atmosphere).

Figure 4 presents the TGA data for the EPDM composite sample. After 20 min of analysis, the TGA curves show, at 200°C, the sample's beginning of mass loss (around 3%). From the temperature of 300 °C, the mass-loss rate is more prominent, reaching the maximum loss rate (83%) at 500°C. From this point, the stabilization of mass loss is established (indicating that all EPDM was consumed), and the SiO_2 present in the composite is maintained (around 17%).

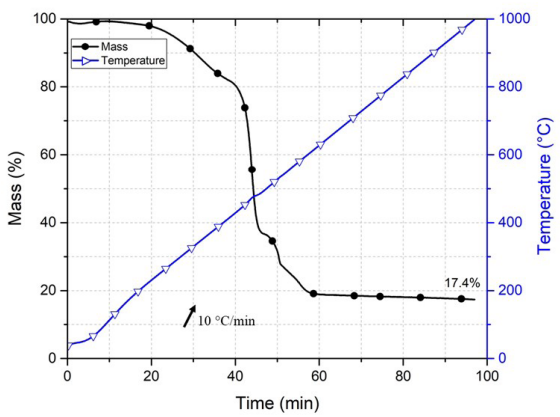

Figure 4. TGA curve of EPDM samples. The temperature varied from 30 to 1000°C, and the heating rate was 10°C/min.

These results make possible the comparison in relation to plasma torch ablation tests. Plasma torch tests provide an environment much closer to the real (of the material application) and how the reinforcement used in the composite helps in its ablative resistance.

3.2. Ablative tests

The following sections will present the results obtained from the ablative tests using a thermal plasma torch.

3.2.1. Morphological analysis of ablated EPDM

Figure 5 shows the images of the control (non-tested) (Figure 5A) and the samples submitted to the ablative tests in different thermal flux: 0.30 MW/m² (Figure 5B), 0.45 MW/m² (Figure 5C), 0.60 MW/m² (Figure 5D), 0.75 MW/m² (Figure 5E) and 0.90 MW/m² (Figure 5F).

The transformations of the characteristics/aspects of the EPDM surface are evident. By observing the sample EPDM1 (Figure 5B) tested under the thermal flux of 0.30 MW/m², layers are formed due to the thermal action with surface wear beginning. From the thermal flux of 0.45 MW/m² (Figure 5C), the char layer begins perceptible, relatively smooth, and compact, and silica precipitates on the surface start to appear, as we can see in the EDS result presented in Figure 6.

Following the increase of the thermal flux, the sample teste under 0.60 MW/m² (Figure 5D) the char is maintained smooth but, in this case, is better distributed on the surface. In the sample EPDM4 (Figure 5E) test under the thermal flux of 0.75 MW/m², the char layer starts to densify, and some pores/holes appear. For 0.90 MW/m² (Figure 5F), the char layer is denser than the other samples; the pores/holes are still present but with less incidence, probably due to the densification of the char. The dense reaction layer is advantageous for ablation resistance[9].

3.2.2. Reaction layer analysis and mass loss rate

The formation of the char reaction layer was investigated to evaluate the performance of the samples under the varied thermal fluxes; for that, the cross-sections also were analyzed by SEM. In Figure 7 are the images of the cross-sections of the samples for all thermal flux.

As observed on the surface of the samples, the densification of the reaction layer occurs; the most interesting is that in the sample tested in higher thermal flux (Figure 7E), the absence of pores or defects is visible.

The dense char layer morphology greatly influences the insulation and ablation performance of the composite: the dense char layer has better mechanical properties, which can improve the resistance of the char layer against erosion by the gas flow and particles[1,21,33].

Under the action of the plasma jet, loss of mass by ablation occurred in the samples.

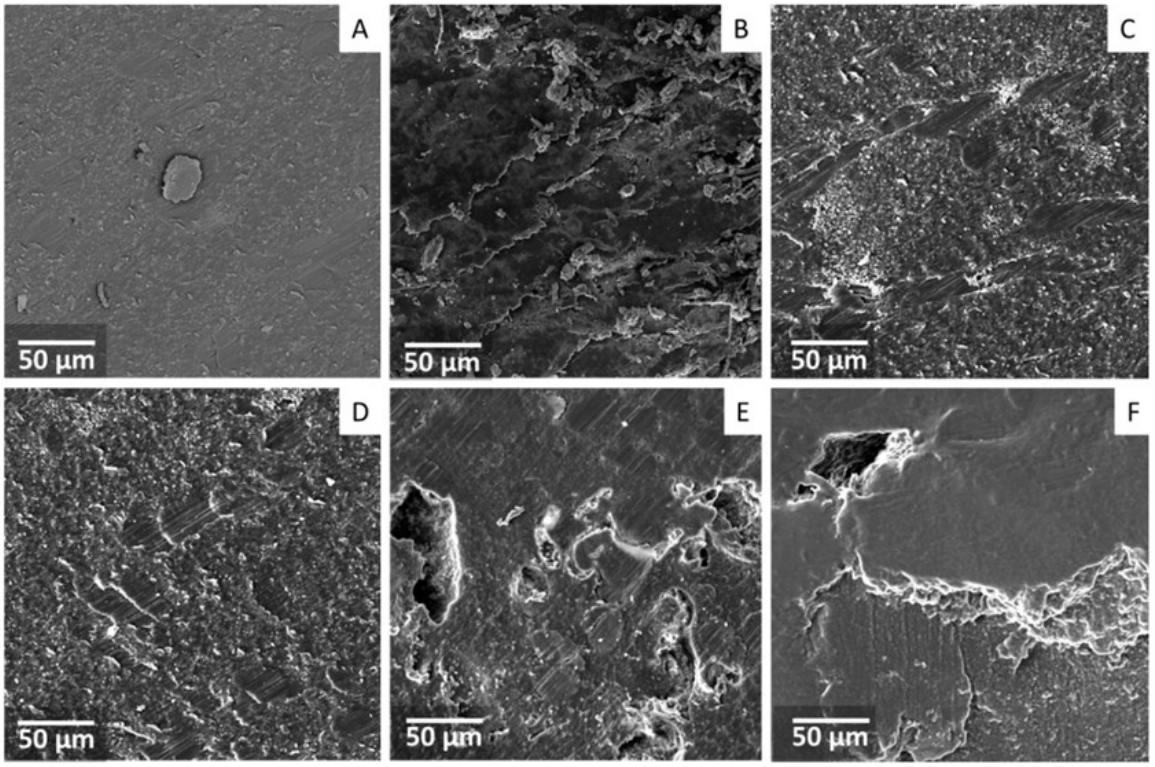

Figure 5. (A) control (non-tested) EPDM 0, (B) EDPM 1 tested under 0.30 MW/m^2, (C) EDPM 2 tested under 0.45 MW/m^2, (D) EDPM 3 tested under 0.60 MW/m^2, (E) EDPM 4 tested under 0.75 MW/m^2, and (F) EDPM 5 tested under 0.90 MW/m^2.

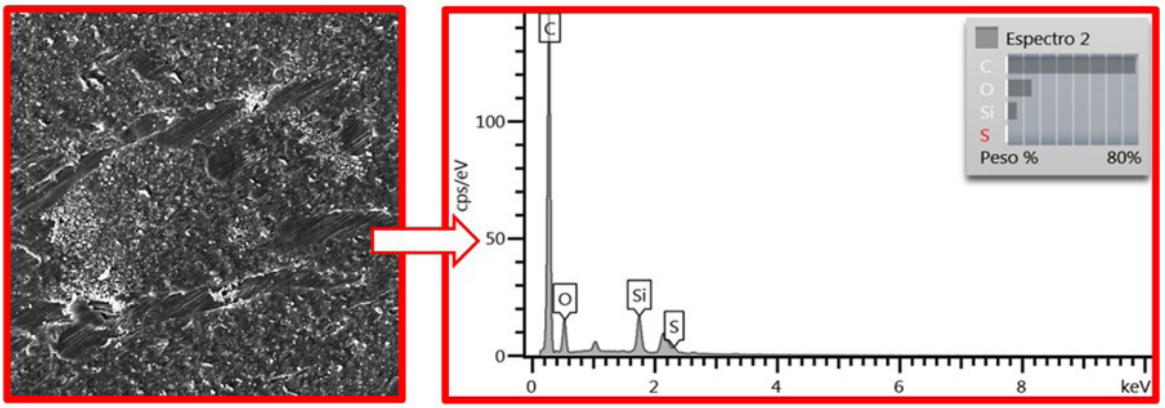

Figure 6. Composition of char layer of ablated EPDM.

The specific mass loss rate " ṁ r " can be calculated according to the expressions:

$$\dot{m} = \frac{m'-m}{S \cdot \Delta t} \quad and \quad S = \frac{1}{4}\pi D^2 \tag{2}$$

where m' and m correspond to sample mass before and after the ablation test, respectively, Δt is the residence time of the sample during the plasma jet, S is the circular area of the sample, and D is the diameter[34].

The mass-loss rate and the width of the formed reaction layer for each sample are presented in Figure 8.

The higher mass loss and formation of the char layer occur for thermal fluxes of 0.3 and 0.45 MW/m^2; from the thermal flux of 0.60 MW/m^2, the mass loss is stable, and probably this result is linked to the formation of the reaction layer (char layer) that minimizes the degradation of the composite. These results could be associated with the initial consumption of the EPDM by the oxidation process. It happens until the char layer is formed, which promotes extra protection of the EPDM, being a barrier to the oxidation process. However, for the highest thermal flux (0.90 MW/m^2), although the loss remained at 5% in relation

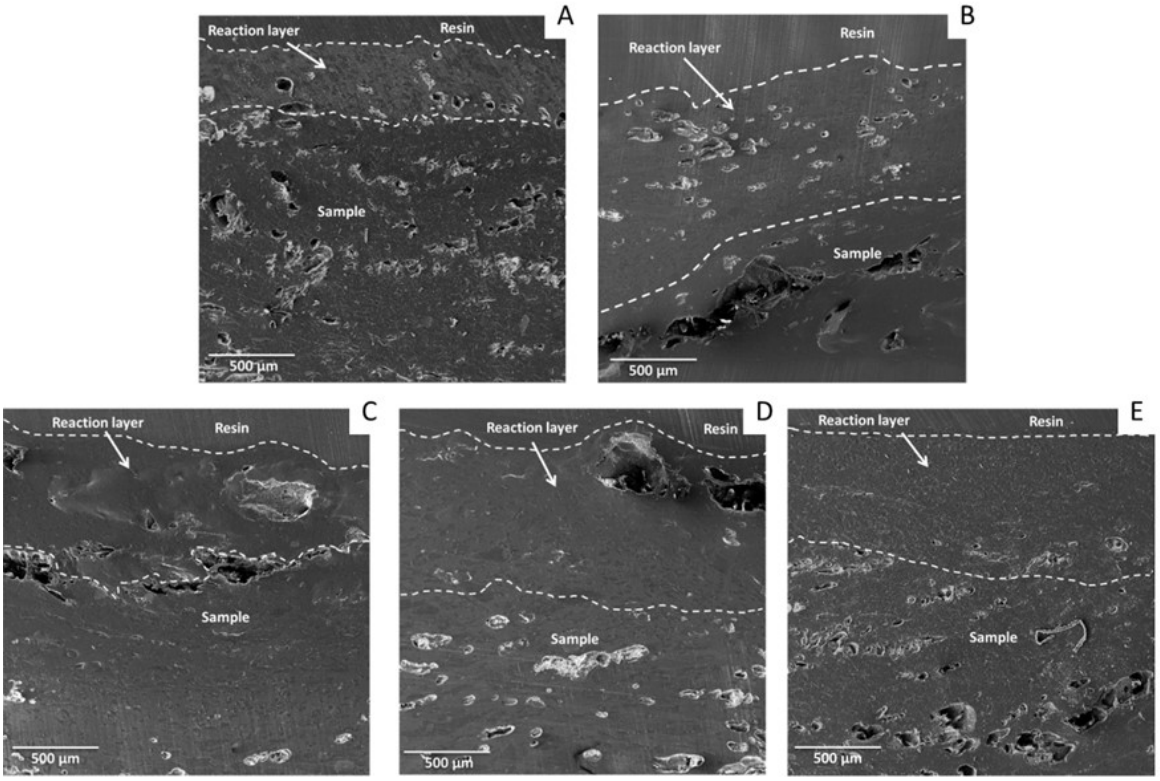

Figure 7. Cross-sections of samples EPDM 1 (A), EPDM 2 (B), EPDM 3 (C), EPDM 4 (D), and EPDM 5 (E).

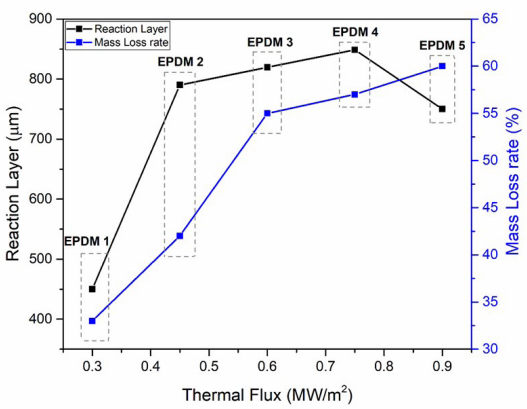

Figure 8. Reaction layer and mass loss evolution.

to the previous thermal flux, the reaction layer starts to be consumed, decreasing the composite protection capacity. Accordingly to Li et al.[1], the mass ablation rate reflects the rate of mass loss of insulation materials during the ablation process, and it is directly linked with the ablation condition and to the overflow rate of the pyrolysis gas. The internal heat (related to the thermal conductivity flux) and the latent heat of pyrolysis influence the reaction layer temperature and, consequently, in the phase transition, thermochemical reaction, and erosion process[1].

Thus, the samples' surface (T-surface) and back (T-back) temperatures were measured to determine the protection and thermal insulation capacity that the reaction layer promotes. Three samples were selected to have an overview of the behaviour of these temperatures, the selected samples were EPDM 1, EPDM 3, and EPDM 5, and the results are shown in Figure 9.

Analyzing the evolution of surface temperatures, an increase in temperature between 1400 and 1600°C is evident. The samples reach the highest surface temperature level around 2s of exposure and remain until the end of the test; when the temperature of the back of the sample is analyzed at around 6s, an exponential increase in temperature occurs. In agreement with the results presented in Figures 7 and 8, when the sample is exposed to the highest thermal flux, 0.9 MW/m^2, it is possible to notice that the surface and back temperature of the sample have the highest values due to the consumption of the reaction layer, such as highlighted earlier. Furthermore, with the measured values, it was possible to determine the thermal diffusivity of the samples EDPM1 (α= 1.04E^{-07} m^2/s), EPDM 3 (α= 1.15E^{-07} m^2/s), and EPDM 5 (α= 1.29E^{-07} m^2/s), the method described by[34].

The FTIR technique was applied to identify the chemical changes in the ablated samples. The FTIR spectra of the control and ablated EPDM samples are shown in Figure 10. Two strong absorption peaks can identify the bands assigned to the C–H stretching vibration at 2920 cm^{-1} (A) and 2850 cm^{-1} (B), and the out-of-plane vibration of CH bonds is attributed to the band located at 721 cm^{-1} (I)[11,35]. The N-H stretching and C- H band vibrations are identified at 1538 cm^{-1} (C) and 1464 cm^{-1} (D), respectively[36]. The peak at 1397 cm^{-1} (E) is

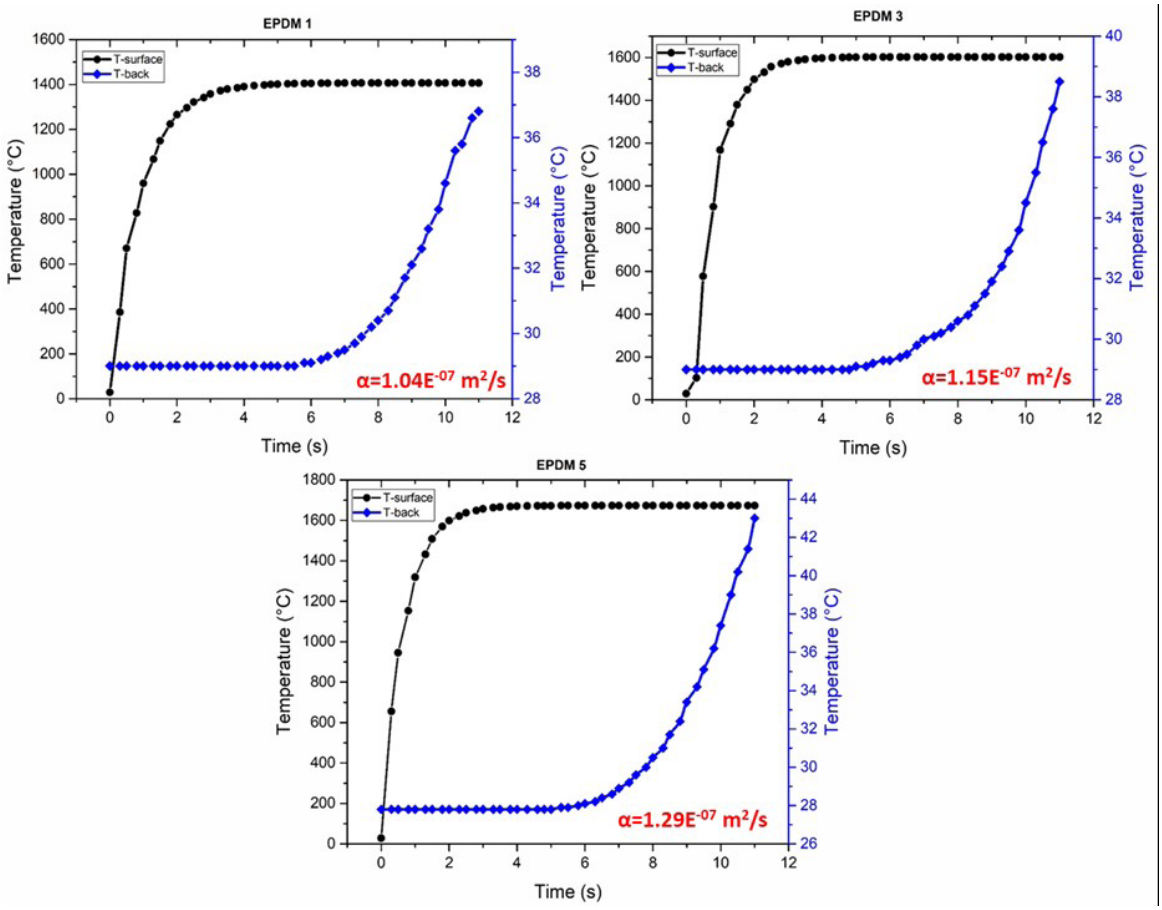

Figure 9. Temperature profile and thermal diffusivity of EPDM 1, EPDM 3, and EPDM 5 samples.

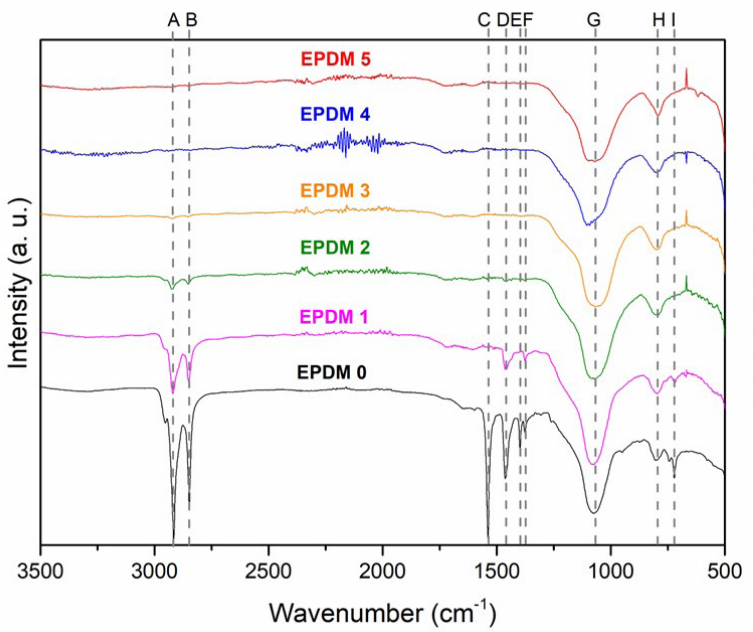

Band	cm^{-1}	Assignment
A	~2920	C-H sym stretching
B	~2850	C-H asym stretching
C	~1538	-NH stretching
D	~1464	C-H band vibrations
E	~1397	CH_3 υsym
F	~1378	CH_3 binding
G	~1076	Si-O-Si stretching
H	~803	Si-O Stretching
I	~721	CH out of plane

Figure 10. FTIR of the control sample (EPDM 0) and the ablated samples EPDM 1, 2, 3, 4, and 5.

assigned to the symmetric CH_3 vibrations, and the peak at 1378 cm^{-1} (F) is assigned to the CH_3 bending. The decrease in intensity of the bands (A, B, C, D, E, and F) could be associated with plasma jet incidence and the oxidation process of the material. The plasma could break the bonds of C-H, N-H, and C-O and promote the thermal oxidation of the material, which are rich in carbon.

The stretching of the Si-O-Si and Si-O groups is identified at 1076 cm^{-1} (G) and 803 cm^{-1} (H), respectively[37].

Analyzing the changes in the spectra, it is possible to identify that the intensity of the peaks related to the CH and NH bond groups lose their intensity from the EPDM 1 sample and disappear entirely in the EPDM 4 and 5 samples. This fact is associated with the Degradation of the EPDM due to intense thermal flux and oxidation provided by the plasma jet. On the other hand, the other bands are consumed right in the first test with lower thermal flux due to the highly oxidative environment that the oxygen plasma jet provides. The addition of silica in EPDM proves effective in containing degradation as it has lower catalyticity and oxygen permeability, causing part of the oxygen to be blocked, preventing it from reaching carbon and, consequently, reducing the material's oxidation. The passivation layer generated by silica is denser, as observed through the SEM (Figure 6); the densification is also associated with reducing the reaction layer, as seen in the graph in Figure 7. However, even with less intensity, there is still a mass loss, but less pronounced.

4. Conclusion

In this work, a thermal plasma-based ablation test system was used to evaluate the ablative performance of the EPDM/Aramid/SiO_2 composite. The samples were submitted to varied thermal fluxes (0.30, 0.45, 0.60, 0.75, and 0.90 MW/m^2) during the exposure time of the 10s. The results show that the evolution of the ablation process, evidenced through the morphological analysis made using the SEM technique, the wear and the formation of the reaction layer becomes perceptible from the thermal flux of 0.45 MW/m^2. The composition and thickness of the char layer were investigated using EDS and FTIR analysis; the ablation process degrades or decomposes most of the components of the composite, remaining just the SiO_2 with predominance. Finally, the mass loss is intense under the thermal fluxes of 0.30 and 0.45 MW/m^2, stabilizing until the 0.75 MW/m^2. The formed char layer begins to lose its protective capacity, evidenced by the decrease in the reaction layer from the thermal flux of 0.90 MW/m2

5. References

1. Li J, Liu K, Guo M, Liu Y, Wang J, Lv X. Ablation and erosion characteristics of EPDM composites under SRM operating conditions. Compos, Part A Appl Sci Manuf. 2018;109:392-401. http://dx.doi.org/10.1016/j.compositesa.2018.03.029.
2. Zhao D, Liu W, Shen Y, Jiang G, Wang T. Improved self-supporting and ceramifiable properties of ceramifiable EPDM composites by adding aramid fiber. Polymers. 2020;12(7):1523. http://dx.doi.org/10.3390/polym12071523.
3. Yezzi C, Moore B. Characterization of Kevlar/EPDM rubbers for use as rocket motor caseinsulators. In: 22nd Joint Propulsion Conference; 1986; Huntsville, AL, USA. Proceedings. Reston: American Institute of Aeronautics and Astronautics; 1986. http://dx.doi.org/10.2514/6.1986-1489.
4. Natali M, Kenny JM, Torre L. Science and technology of polymeric ablative materials for thermal protection systems and propulsion devices: a review. Prog Mater Sci. 2016;84:192-275. http://dx.doi.org/10.1016/j.pmatsci.2016.08.003.
5. Sugama T, Pyatina T, Redline E, McElhanon J, Blankenship D. Degradation of different elastomeric polymers in simulated geothermal environments at 300°C. Polym Degrad Stabil. 2015;120:328-39. http://dx.doi.org/10.1016/j.polymdegradstab.2015.07.010.
6. Xu Y, Hu C, Zeng Z, Yang YX. Research on mechanical model of EPDM insulation charring layer. Appl Mech Mater. 2012;152–154:57-63. http://dx.doi.org/10.4028/www.scientific.net/AMM.152-154.57.
7. Rallini M, Puri I, Torre L, Natali M. Boron based fillers as char enhancers of EPDM based heat shielding materials for SRMs: A comparative analysis. Compos Struct. 2018;198:73-83. http://dx.doi.org/10.1016/j.compstruct.2018.03.102.
8. Mokhothu TH, Luyt AS, Messori M. Reinforcement of EPDM rubber with in situ generated silica particles in the presence of a coupling agent via a sol-gel route. Polym Test. 2014;33:97-106. http://dx.doi.org/10.1016/j.polymertesting.2013.11.009.
9. Guo M, Li J, Xi K, Liu Y, Ji J. Effect of multi-walled carbon nanotubes on thermal stability and ablation properties of EPDM insulation materials for solid rocket motors. Acta Astronaut. 2019;159:508-16. http://dx.doi.org/10.1016/j.actaastro.2019.01.047.
10. Jiang X, Zhang Y, Zhang Y. Study of dynamically cured PP/MAH-g-EPDM/epoxy blends. Polym Test. 2004;23(3):259-66. http://dx.doi.org/10.1016/j.polymertesting.2003.08.004.
11. Singh S, Guchhait PK, Bandyopadhyay GG, Chaki TK. Development of polyimide-nanosilica filled EPDM based light rocket motor insulator compound: influence of polyimide-nanosilica loading on thermal, ablation, and mechanical properties. Compos, Part A Appl Sci Manuf. 2013;44:8-15. http://dx.doi.org/10.1016/j.compositesa.2012.08.016.
12. Saha Deuri A, Bhowmick AK, Ghosh R, John B, Sriram T, De SK. Thermal and ablative properties of rocket insulator compound based on EPDM. Polym Degrad Stabil. 1988;21(1):21-8. http://dx.doi.org/10.1016/0141-3910(88)90062-6.
13. Jia X, Zeng Z, Li G, Hui D, Yang X, Wang S. Enhancement of ablative and interfacial bonding properties of EPDM composites by incorporating epoxy phenolic resin. Compos, Part B Eng. 2013;54:234-40. http://dx.doi.org/10.1016/j.compositesb.2013.05.005.
14. Rallini M, Puri I, Torre L, Natali M. Thermal and ablation properties of EPDM based heat shielding materials modified with density reducer fillers. Compos, Part A Appl Sci Manuf. 2018;112:71-80. http://dx.doi.org/10.1016/j.compositesa.2018.05.031.
15. Chen Y, Chen P, Hong C, Zhang B, Hui D. Improved ablation resistance of carbon-phenolic composites by introducing zirconium diboride particles. Compos, Part B Eng. 2013;47:320-5. http://dx.doi.org/10.1016/j.compositesb.2012.11.007.
16. Kong L, Zuo X, Zhu S, Li Z, Shi J, Li L, et al. Novel carbon-poly(silacetylene) composites as advanced thermal protection material in aerospace applications. Compos Sci Technol. 2018;162:163-9. http://dx.doi.org/10.1016/j.compscitech.2018.04.038.
17. Pulci G, Tirillò J, Marra F, Fossati F, Bartuli C, Valente T. Carbon-phenolic ablative materials for re-entry space vehicles: manufacturing and properties. Compos, Part A Appl Sci Manuf. 2010;41(10):1483-90. http://dx.doi.org/10.1016/j.compositesa.2010.06.010.
18. Gao G, Zhang Z, Zheng Y, Jin Z. Effect of fiber orientation angle on thermal Degradation and ablative properties of short-fiber reinforced EPDM/NBR rubber composites. Polym Compos. 2009;16:NA. http://dx.doi.org/10.1002/pc.20909.
19. Kim JS, Bae JW, Lee JH, Lee Y-H, Kim H-D. Preparation and properties of high-performance recyclable ethylene propylene

diene rubber. J Appl Polym Sci. 2015;132(44):1-9. http://dx.doi.org/10.1002/app.42718.
20. Jaramillo M, Koo JH, Natali M. Compressive char strength of thermoplastic polyurethane elastomer nanocomposites. Polym Adv Technol. 2014;25(7):742-51. http://dx.doi.org/10.1002/pat.3287.
21. Li J, Xi K, Lv X, Li Q, Wang S. Characteristics and formation mechanism of compact/porous structures in char layers of EPDM insulation materials. Carbon. 2018;127:498-509. http://dx.doi.org/10.1016/j.carbon.2017.10.091.
22. Nakamura T, Chaikumpollert O, Yamamoto Y, Ohtake Y, Kawahara S. Degradation of EPDM seal used for water supplying system. Polym Degrad Stabil. 2011;96(7):1236-41. http://dx.doi.org/10.1016/j.polymdegradstab.2011.04.007.
23. Ji Y, Han S, Xia L, Li C, Wu H, Guo S, et al. Synergetic effect of aramid fiber and carbon fiber to enhance ablative resistance of EPDM-based insulators via constructing high-strength char layer. Compos Sci Technol. 2021;201:108494. http://dx.doi.org/10.1016/j.compscitech.2020.108494.
24. Miranda FS, Caliari FR, Campos TM, Essiptchouk AM, Petraconi G Fo. Deposition of graded SiO_2/SiC coatings using high-velocity solution plasma spray. Ceram Int. 2017;43(18):16416-23. http://dx.doi.org/10.1016/j.ceramint.2017.09.018.
25. Haibo O, Cuiyan L, Jianfeng H, Liyun C, Jie F, Jing L, et al. Self-healing ZrB2-SiO2 oxidation resistance coating for SiC coated carbon/carbon composites. Corros Sci. 2016;110:265-72. http://dx.doi.org/10.1016/j.corsci.2016.04.040.
26. Wang Y, Chen Z, Yu S. Ablation behavior and mechanism analysis of C/SiC composites. J Mater Res Technol. 2016;5(2):170-82. http://dx.doi.org/10.1016/j.jmrt.2015.10.004.
27. García E, Nistal A, Martín de la Escalera F, Khalifa A, Sainz MA, Osendi MI, et al. Thermally sprayed Y_2O_3-Al_2O_3-SiO_2 coatings for high-temperature protection of SiC ceramics. J Therm Spray Technol. 2014;24:185-93. http://dx.doi.org/10.1007/s11666-014-0178-y.
28. Charakhovski L, Silva WG, Essiptchouk AM, Petraconi G, Barros EA, Maciel HS, et al. Hypersonic and subsonic plasma setups for testing heat shielding materials. In: 12th Brazilian Congress of Thermal Engineering and Sciences; 2008; Belo Horizonte. Proceedings. Rio de Janeiro: ABCM; 2008.
29. Petraconi G, Essiptchouk AM, Charakhovski LI, Otani C, Maciel HS, Pessoa RS, et al. Degradation of carbon-based materials under ablative conditions produced by a high enthalpy plasma jet. J Aerosp Technol Manag. 2010;2(1):33-40. http://dx.doi.org/10.5028/jatm.2010.02013340.
30. Paterniani Rita CC, Miranda FS, Caliari FR, Rocha R, Essiptchouk A, Charakhovski L, et al. Hypersonic plasma setup for oxidation testing of ultrahigh temperature ceramic composites. J Heat Transfer. 2020;142(8):082103. http://dx.doi.org/10.1115/1.4047150.
31. Samal S. Thermal plasma technology: the prospective future in material processing. J Clean Prod. 2017;142:3131-50. http://dx.doi.org/10.1016/j.jclepro.2016.10.154.
32. Boulos MI, Fauchais P, Pfender E. Thermal plasma fundamentals and applications. 1st ed. New York: Springer Science+Business Media, LLC; 1994.
33. Li J, Guo M, Lv X, Liu Y, Xi K, Guan Y. Erosion characteristics of ethylene propylene diene monomer composite insulation by high-temperature dense particles. Acta Astronaut. 2018;145:293-303. http://dx.doi.org/10.1016/j.actaastro.2018.01.055.
34. Silva RJ, Reis RI, Pardini LC, Sias DF, Filho GP. Low-energy ablation and low thermal diffusivity of a CFRC composite modified by SiC. Int J Thermophys. 2019;40(10):88. http://dx.doi.org/10.1007/s10765-019-2555-8.
35. Vadivel M, Kumar MSC, Mohaideen JA, Alagar M, Sankarganesh M, Raja JD. Hybrid siliconized–epoxidized EPDM/polyurethane (eEPDM-g-APTES/HTPDMS/PU) matrices for potential application in cable insulation. Polym Polymer Compos. 2020;28(8-9):589-97. http://dx.doi.org/10.1177/0967391119894169.
36. Jović B, Panić M, Radnović N, Živojević K, Mladenović M, Crnojević V, et al. Investigation of the surface interactions of selected amides with mesoporous silica using FTIR spectroscopy and hyperspectral imaging. J Mol Struct. 2020;1219:128562. http://dx.doi.org/10.1016/j.molstruc.2020.128562.
37. Miranda FS, Caliari FR, Campos TM, Leite DMG, Pessoa RS, Essiptchouk AM, et al. High-velocity plasma spray process using hybrid SiO_2 + ZrO_2 precursor for deposition of environmental barrier coatings. Surf Coat Tech. 2020;404:126447. http://dx.doi.org/10.1016/j.surfcoat.2020.126447.